Upper Critical Solution Temperature Phase Behavior, Composition Fluctuations, and Complex Formation in Poly (Vinyl Methyl Ether)/D_2O Solutions: Small-Angle Neutron-Scattering Experiments and Wertheim Lattice Thermodynamic Perturbation Theory Predictions

Erik Nies,*,†,‡ Ting Li,‡,§ Hugo Berghmans,‡ Richard K. Heenan,|| and Stephen M. King||

Laboratory of Polymer Technology, Eindhoven University of Technology, P.O. Box 513, 5600MB Eindhoven, The Netherlands, Polymer Research Division, Department of Chemistry, Katholieke Universiteit Leuven, Celestijnenlaan 200F, B-3001 Heverlee, Belgium, State Key Laboratory of Polymer Physics & Chemistry, Center for Molecular Science, Institute of Chemistry, Chinese Academy of Sciences, Zhongguancun, Beijing 100080, Peoples' Republic of China, and ISIS Facility, Rutherford Appleton Laboratory, Chilton, Didcot, Oxfordshire OX1 0QX, UK

Received: October 7, 2005; In Final Form: January 16, 2006

Small-angle neutron-scattering measurements are presented for homogeneous mixtures of poly (methyl vinyl ether) (PVME) and deuterium oxide (D_2O) at high polymer concentrations and for temperatures lower than the equilibrium melting point of the solvent. The experimental data are analyzed to give values for the second-order compositional derivative of the Gibbs energy and the Ornstein−Zernike correlation length. The experimental data together with earlier SANS data determined at higher temperatures cannot be represented with an extended Flory−Huggins (F−H) interaction function depending on composition and temperatures. The experimental data confirm the existence of a narrow upper critical solution temperature (UCST) miscibility gap at high concentrations in agreement with theoretical predictions of the Wertheim lattice thermodynamic perturbation theory (LTPT). The Wertheim LTPT incorporates the influence of hydrogen bonding and predicts not only the existence of bimodal lower critical solution temperature (LCST) phase behavior but also the occurrence of highly unconventional *two narrow adjacent UCST miscibility gaps.* Finally, the experimental data do not support the existence of a stable molecular complex at the investigated temperatures and compositions. Even at the lowest investigated temperature, the energy required to induce typical Ornstein−Zernike-like concentration fluctuations is smaller than the thermal energy. Also, in this case, the Wertheim LTPT provides a theoretical basis to understand the formation of polymer solvent associations in PVME/water.

Introduction

Aqueous solutions of poly (methyl vinyl ether) (PVME) exhibit a wide lower critical solution temperature (LCST) miscibility gap nearly covering the full composition range.[1,2] The occurrence of an LCST miscibility gap is not really surprising, as it is characteristic of polymer solutions that exhibit hydrogen bonding. In these polymer solutions and small molecule mixtures alike, orientation-dependent or saturation interactions play a key factor in the occurrence of LCST and closed loop phase behavior and lead to flat and wide LCST miscibility gaps encompassing the largest part of the composition range.[3−6] What is unusual about the LCST phase behavior in PVME/deuterium oxide (D_2O) and PVME/H_2O is the bimodality of the liquid−liquid (L−L) miscibility gap[1,7,8] with two stable critical points.[9]

Apart from the peculiar "high temperature" phase behavior, aqueous mixtures of PVME cease to crystallize at sufficiently high polymer concentration.[10,11] This has been interpreted to point to the existence of a polymer/solvent complex in which water molecules are tightly bound to the polymer chain. Depending on the investigated property, polymer/water complexes containing from 2 up to 5 molecules of water have been suggested.[10,12,13]

In a previous contribution, small-angle neutron-scattering (SANS) measurements were presented as a function of temperature and composition for homogeneous mixtures of poly (methyl vinyl ether) and D_2O bounded by the bimodal LCST at high temperature and by the equilibrium melting temperature of D_2O at low temperature.[8] These experimental data were used to obtain values for the parameters in an extended Flory−Huggins (F−H) interaction function linear in temperature and cubic in composition. Using the extended interaction function, the predicted LCST miscibility behavior was in qualitative agreement with the experimental data, and importantly, the remarkable bimodal phase behavior was recovered in the calculations. Moreover, it was concluded that the experimental data do not support the existence of a stable molecular complex at the investigated temperatures and compositions, as the mixtures are characterized by Ornstein−Zernike-like composition fluctuations. On the other hand, the experiments showed that, with decreasing temperature, the amplitude of the spontaneous concentration fluctuations is reduced, but even at the lowest investigated temperature, ca. 10 °C, the energy required

* To whom correspondence should be addressed. E-mail: e.l.f.nies@tue.nl.
† Eindhoven University of Technology.
‡ Katholieke Universiteit Leuven.
§ Chinese Academy of Sciences.
|| ISIS Facility.

10.1021/jp055718l CCC: $33.50
Published on Web 03/01/2006

to induce typical Ornstein−Zernike-like concentration fluctuations is still smaller than the thermal energy.

SANS provides a unique opportunity to investigate the thermal (composition) fluctuations and the presence of association and even complexation. In this contribution, we report on SANS measurements of PVME/D_2O mixtures extending to temperatures lower than the equilibrium melting temperature of D_2O. Measurements at lower temperatures are possible for highly concentrated mixtures, as the crystallization of D_2O at high polymer concentrations occurs at lower temperatures, due to the classical melting point depression effect, or does not occur at all at sufficiently high polymer composition.

We also present a theoretical approach that explicitly incorporates the formation of hydrogen-bonding interactions. We base our approach on the thermodynamic perturbation theory of Wertheim[14,15] concerning saturation interactions mapped onto the lattice.[16] The theory will be used to give a qualitative interpretation of the observed phase behavior and neutron-scattering composition fluctuations.

In the next section, chemicals and experimental techniques are described. In the theoretical section, the relationship between SANS scattering cross sections, concentration fluctuation theory, and thermodynamic properties is briefly highlighted. The basic equations of the lattice theory are provided. The results of the current investigation are presented and discussed in the section Results and Discussion, and finally, some conclusions are presented.

Experimental Section

Materials and Mixtures Preparation. D_2O (purity 99.95%), purchased from Merck, was used without further purification. Poly (vinyl methyl ether) (PVME, $(CH_2CHOCH_3)_n$), dissolved in water (mass fraction of PVME, $w_{PVME} = 0.5$), was purchased from Sigma-Aldrich. The mixture was diluted to $w_{PVME} = 0.1$ and heated to ca. 50 °C to induce liquid−liquid-phase separation. The phase lean in polymer was removed, and the phase rich in polymer was dried at 60 °C under vacuum for 2 days. The dried PVME was used in the further preparation of polymer mixtures with D_2O.

In the composition range $0.1 \leq w_{PMVE} \leq 0.9$, mixtures of PVME and D_2O were prepared by adding appropriate amounts of polymer and solvent. Mixture compositions were expressed in PVME mass fraction w_{PVME}. These mixtures were allowed to homogenize at room temperatures in closed recipients for periods up to two months for the highest polymer concentrations. The mixtures were regularly mechanically mixed in the recipient.

Small-Angle Neutron-Scattering (SANS) Measurements. Small-angle neutron-scattering (SANS) experiments were performed on the LOQ instrument at the ISIS pulsed neutron source, Rutherford Appleton Laboratory, Didcot, UK.[17] The range of wavelengths used was $2.2\ \text{Å} \leq \lambda \leq 10\ \text{Å}$ at 25 Hz, corresponding to a range in scattering vector magnitude $q = 4\pi \sin(\theta/2)/\lambda$, where θ is the scattering angle of $0.006\ \text{Å}^{-1} \leq q \leq 1.49\ \text{Å}^{-1}$. The beam size at the sample was collimated to 10-mm diameter. Scattering neutrons were recorded simultaneously on two two-dimensional (2D) detectors with different angular coverage (details about the detectors can be found in ref 17).

Fluid samples were contained in quartz glass cuvettes (purchased from Starna and Hellma), whereas the highly viscous concentrated mixtures were placed in demountable but sealed cells. Both types of cell had a path length of 1 mm to reduce incoherent scattering effects from the hydrogen atoms in the polymer. SANS data were collected as a function of mixture composition (including pure D_2O and pure PVME) and temperature. The measurement time at each temperature was 1 h, and after attaining a new measuring temperature, an equilibration time of ca. 20 min was allowed. In the temperature interval 10−20 °C, temperature control was achieved by means of a circulating fluid bath (standard sample environment on LOQ). In the lower temperature interval −20− 45 °C, data were obtained in a helium cryostat. Details of both sample environments are described elsewhere.[18]

The raw scattering data were treated according to standard procedures using the instrument-specific "COLETTE" data reduction program developed at ISIS.[19] Raw data were divided by the monitor count, sample thickness, and the measured sample transmission and corrected for detector efficiency. Differential scattering cross sections, expressed in cm^{-1}, were then obtained by circularly averaging the isotropic scattering datasets. The data were placed on an absolute scale by reference to the scattering from a calibration standard (the details of which are discussed in Appendix 4 in ref 19). Subsequently, similarly treated scattering cross-section data recorded from the empty sample container were subtracted from the sample scattering data.

Theoretical section

Scattering Cross Sections due to Concentration Fluctuations. The measured absolute scattering cross sections of the samples contain an incoherent contribution carrying no structural information and coherent contributions due to density fluctuations and concentration fluctuations. To obtain the scattering related to the concentration fluctuations in binary mixtures of solvent and polymer (PVME), the incoherent scattering largely caused by the hydrogenated material and the coherent scattering caused by density fluctuations is removed from the measured signal by subtracting the scattering of the pure components in the appropriate volume ratio.[20]

$$\frac{\partial\sigma}{\partial\Omega}(q)|_{conc} = \frac{\partial\sigma}{\partial\Omega}(q)|_{observed} - \phi_{solvent}\frac{\partial\sigma}{\partial\Omega}(q)|_{solvent} - \phi_{PVME}\frac{\partial\sigma}{\partial\Omega}(q)|_{PVME} \quad (1)$$

where $\partial\sigma/\partial\Omega(q)|_X$ is the absolute coherent scattering cross section due to concentration fluctuations (X = conc), the observed scattering cross section (X = observed), the observed scattering cross section of the solvent ($X = D_2O$) and of PVME (X = PVME), and ϕ_i is the volume fraction of component i in the mixture. The volume fractions of the mixture components are calculated from the mass fraction with the assumption that mixing is not accompanied by volume changes.[8]

The subtraction in eq 1 will not be perfect due to experimental uncertainties in the scattered intensities and in the volume fractions, and a residual background signal may remain; hence, the experimental scattering cross section is presented by

$$\frac{\partial\sigma}{\partial\Omega}(q)|_{conc,exp} = \frac{\partial\sigma}{\partial\Omega}(q)|_{conc} + B \quad (2)$$

where B is a residual q-independent background intensity.

Scattering Cross Section from Concentration Fluctuation Theory. According to the concentration fluctuations theory initiated by Smoluchowski,[21] Einstein,[22] and Debye,[23] the absolute scattering cross section due to concentration fluctuations

in a binary mixture is given by[20,23,24]

$$\frac{\partial\sigma}{\partial\Omega}(q)|_{\text{conc}} = \frac{\frac{\partial\sigma}{\partial\Omega}(q=0)|_{\text{conc}}}{(1+(\xi q)^2)} = \frac{\bar{b}^2}{V_0}\frac{\left(\frac{\partial^2\Delta G/(NkT)}{\partial\phi_1^2}\right)^{-1}}{(1+(\xi q)^2)} \quad (3)$$

with $\partial\sigma/\partial\Omega\ (q=0)|_{\text{conc}}$ being the scattering cross section in the forward direction, and ξ is the correlation length [Å], V_u is the volume of the unit cell, V_0 (V_1) is the volume of a molecule of the solvent (component 0) (polymer, component 1), b_0 (b_1) the neutron-scattering length of species 0 (1), $\Delta G/N$ is the free enthalpy of mixing per unit cell, N is the number of unit cells, k is Boltzmann's constant, T is the absolute temperature, and $\bar{b} = V_u(b_0/V_0 - b_1/V_1)$ is the contrast factor.[8,24,25]

Spinodal Conditions and Scattered Intensity. At the stability limit or spinodal condition, the curvature of the Gibbs energy becomes zero.[26] Ignoring the gradient energy contribution and nonclassical behavior, which both only become important very close to the stability limit,[23] a mean field estimate of the spinodal temperature at a particular composition can be determined from the extrapolation as a function of the temperature (or inverse temperature) of $((\partial^2\Delta G/NkT)/\partial\phi_1^2)$ to zero value.

Theoretical Models for the Gibbs Energy of Mixing Expressions. Further information about the thermodynamics can be obtained when we use a specific theoretical model for the Gibbs energy. In earlier work, we adopted the classic F−H lattice theory expression for the Gibbs energy amended with an interaction function dependent on temperature and mixture composition.[9,26]

The Amended Flory−Huggins Gibbs Energy of Mixing Expression. The main equation of this theory describes the free enthalpy of mixing per lattice site (unit cell) of two monodisperse components as follows:

$$\frac{\Delta G}{NkT} = \frac{\phi_0}{s_0}\ln\phi_0 + \frac{\phi_1}{s_1}\ln\phi_1 + \Gamma(\phi_1,T) = \frac{\phi_0}{s_0}\ln\phi_0 + \frac{\phi_1}{s_1}\ln\phi_1 + \phi_0\phi_1 g(\phi_1,T) \quad (4)$$

where $\phi_1(\phi_0)$ is the volume fraction of polymer (solvent), s_1 (s_0) is the relative chain length or number of unit lattice cells taken by a molecule of component 1 (0), $\Gamma(\phi_1,T)$ is the F−H interaction function, and $g(\phi_1,T)$, the extended F−H interaction parameter defined by the second equality, is assumed to be a polynomial in concentration and temperature. The relative chain lengths s_i in eq 4 are calculated from $s_i = M_i/\rho_i V_l N_A$ where M_i is the molar mass, ρ_i is the density of component i, V_l is the volume of a lattice unit cell, and N_A is Avogadro's number.

To describe the SANS data covering the whole composition range, a cubic polynomial function will be used, as in earlier work[8] with

$$g(\phi_1,T) = \sum_{l=0}^{l_{max}=3} g_l(T)\phi_1^l \quad (5a)$$

$$g_l = g_{l0} + g_{l1}/T + g_{l2}T \quad (5b)$$

and g_{l0}, g_{l1}, and g_{l2} are constants.

A Wertheim Lattice Thermodynamic Perturbation Theory. From the theoretical point of view, it is of interest to understand the complicated phase behavior and the detailed information obtained from the SANS scattering experiments using a theoretical approach that incorporates directly and explicitly the formation of hydrogen-bonding interactions. We do a first attempt and follow the seminal work of Wertheim concerning saturation interactions.[14,15] We mapped the Wertheim theory onto the fully occupied lattice model[16] that is also the basis for the F−H theory[27,28] and use the theory to study the phase behavior of a model polymer solution that involves specific interactions between solvent molecules and between polymer segments and solvent molecules. Details of the theory are presented elsewhere,[16] and we only summarize the model parameters and the equations needed to calculate the L−L spinodal and critical conditions here.

The lattice positions, N_L in total, have coordination number z and are occupied either by a solvent molecule (component 0) or by a segment of a polymer molecule (component 1). Each molecule of component 0 carries a specific site A, and each segment of component 1 carries a specific site B. By the attachment of the specific sites A and B, the molecules of 0 and segments of 1, respectively, acquire orientational degrees of freedom. Nearest-neighbor molecules and segments interact by dispersive interactions with an interaction energy, $-\epsilon_{ij}$ ($i,j = 0,1$), depending on the pair of units (solvent molecules or polymer segments) involved. Furthermore, the specific sites A on molecules of type 1 interact with interaction strength $-\epsilon_{00}^{AA}$ if they are properly oriented relative to each other, and specific sites A and B interact with interaction strength $-\epsilon_{01}^{AB} = -\epsilon_{10}^{BA}$ if they are properly oriented relative to each other. We do not have a specific interaction between sites B because the polymer cannot self associate, i.e., $\epsilon_{11}^{BB} = 0$.

For the fully occupied lattice model, no excess volume contributions occur, and the excess Helmholtz energy $\Delta A/N_L$ is equal to the excess Gibbs energy $\Delta G/N_L$, defined as

$$\Delta G/N_L = G/N_L - \phi_0 G_0/N_{L0} - \phi_1 G_1/N_{L1} \quad (6)$$

where G_i/N_{Li} is the Gibbs energy per lattice site for pure component i and ϕ_i is the lattice site fraction (or volume fraction) of component i. An equation similar to eq 6 applies for the excess Helmholtz energy.

In the thermodynamic perturbation theory of Wertheim, the excess Gibbs energy per lattice site can be written as a sum, according to

$$\Delta G/N_L kT = \Delta G_R/N_L kT + \Delta G_{NN}/N_L kT + \Delta G_{AB}/N_L kT \quad (7)$$

The excess Gibbs energy of the reference system ΔG_R is the Gibbs energy of the same system excluding both nearest-neighbor and specific interactions, and in the Wertheim lattice thermodynamic perturbation theory (LTPT), the F−H combinatorial entropy is recovered.

$$\frac{\Delta G_R}{N_L kT} = \frac{\phi_0}{s_0}\ln\phi_0 + \frac{\phi_1}{s_1}\ln\phi_1 \quad (8)$$

with s_i being the number of lattice sites occupied by a molecule of type i.

For the excess free enthalpy of nearest-neighbor interactions, the following mean field approximation is used

$$\frac{\Delta G_{NN}}{N_L kT} = \frac{z\Delta w}{2kT}\phi_0\phi_1 = \chi\phi_0\phi_1 \quad (9)$$

where χ is the F−H interaction parameter, z is the lattice coordination number, and $\Delta w = 2(-\epsilon_{01}) - ((-\epsilon_{00}) + (-\epsilon_{11}))$ is the exchange energy defined for the nearest-neighbor dispersive interactions, which is in the F−H theory as the only relevant energy scale. The F−H exchange energy can also be

used to define a reduced temperature $T^* = 2kT/z\Delta w$, which will be used in the calculations and the presentations of the predictions.

The sum of eqs 8 and 9 constitute the standard F−H mixture or solution theory in its simplest mean field approximation. It does not provide a quantitative prediction of the true phase behavior of the model but does capture its essence.

The excess free enthalpy due to the association between A sites and A and B sites is given by

$$\frac{\Delta G_{AB}}{N_L kT} = \phi_0\left[\ln X_A^0 - \frac{X_A^0}{2} + \frac{1}{2}\right] + \phi_1\left[\ln X_B^1 - \frac{X_B^1}{2} + \frac{1}{2}\right] \qquad (10)$$

with X_A^0 (X_B^1) being the fraction of nonbonded site A (B).

The nonbonded fractions are determined from the set of equations:

$$\bar{X}_A(1 + \bar{X}_A\Delta_{AA} + \bar{X}_B\Delta_{AB}) - \phi_0 = 0$$

and

$$\bar{X}_B(1 + \bar{X}_A\Delta_{AB}) - \phi_1 = 0 \qquad (11)$$

with $\bar{X}_A = \phi_0 X_A^0$ and $\bar{X}_B = \phi_1 X_B^1$.

The parameters $\Delta_{\alpha\beta}$ (α, β = A or B) in eqs 11 are given by

$$\Delta_{\alpha\beta} = K(\exp(\epsilon_{ij}^{\alpha\beta}/k_B T) - 1) \qquad (12)$$

with K being the ratio of the nearest-neighbor positions with the proper orientation to all possible orientations.

From the excess Gibbs energy, eq 7, other thermodynamic properties are easily obtained. In particular, spinodal and critical conditions can be calculated from the second and third compositional derivative of the Gibbs energy

$$J_{sp} = \left.\frac{\partial^2 \Delta G/NkT}{\partial \phi_1^2}\right|_{T,p}$$

and

$$J_{cr} = \left.\frac{\partial^3 \Delta G/NkT}{\partial \phi_1^3}\right|_{T,p} \qquad (13)$$

At the spinodal, only $J_{sp} = 0$ is obeyed. The critical temperature and composition are given by the simultaneous set of equations $J_{sp} = 0$ and $J_{cr} = 0$.

Results and Discussion

Concentrated Mixtures of PVME/D_2O. *Experimental SANS Scattering Cross Sections.* Several compositions of PVME in D_2O covering the whole concentration range $0.1 \le w_{PVME} \le 0.9$ were measured at different temperatures ranging from ca. −40 to +10 °C. All experimental scattering data were analyzed using the Ornstein−Zernike (OZ)-equation (eq 3) and the forward-scattered intensity $\partial\sigma/\partial\Omega(q = 0)|_{conc}$; the correlation length ξ and the residual background B were determined at each composition and temperature. In Figure 1, a typical example is presented of the scattering cross sections due to concentration fluctuations for a mixture with $w_{PVME} \cong 0.8$. The experimental data are accurately fitted by the OZ-equation, eq 3, for concentration fluctuations. The change in the statistical quality of the data at $q \approx 0.2$ Å^{-1} represents the overlap in q between the two detectors.

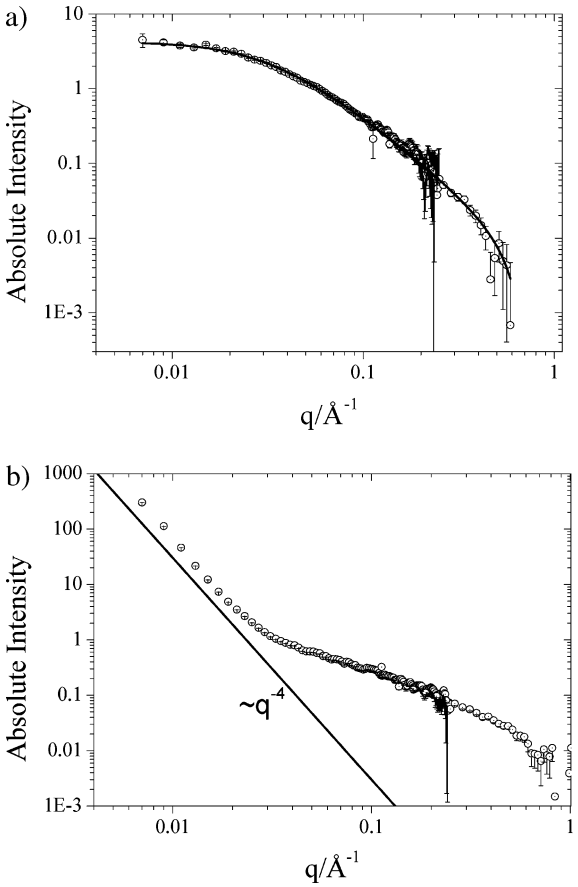

Figure 1. Plot of the scattering cross section $(\partial\sigma/\partial\Omega)(q)|_{conc,exp}$ (○) and estimated experimental uncertainties vs q. (a) Plot for PVME/D_2O $w_{PVME} = 0.795$ at $T = 0.1$ °C. The solid line is the result of the fit of the experimental data to the Ornstein Zernike equation, eq 3. (b) Plot for PVME/D_2O $w_{PVME} = 0.762$ at $T = -42.0$ °C. The straight line shows the q^{-4} dependence at small q.

Spinodal Conditions. Independent of a model for the Gibbs energy (of mixing), the spinodal temperatures can be determined from the forward-scattering cross sections. For each concentration, the values of $(\partial^2\Delta G/NkT/\partial\phi_1^2)$ (denoted as G''/kT) (or $((\partial\sigma/\partial\Omega)(q = 0)|_{conc})^{-1}$) are plotted versus T, as presented in Figure 2.

For the lower compositions ($0 \le w_{PVME} \le 0.6$) depicted in Figure 2a, the curvature of the Gibbs energy of mixing monotonically decreases with increasing temperature. This points to the existence of LCST spinodal temperatures, as already discussed.[8] Due to the interference of the crystallization of D_2O from the mixtures, we cannot measure the equilibrium concentration fluctuations for $T \le 275$ K at these concentrations.

At higher concentrations ($w_{PVME} \ge 0.7$, see Figure 2b), the data do not vary with temperature in the same way. In the composition interval $0.7 \le w_{PVME} \le 0.8$, the curvature of the Gibbs energy reaches a maximum at intermediate temperatures and decreases both at low and high temperatures. For sufficiently high compositions $w_{PVME} > 0.88$, only a monotonic increase with temperature of $(\partial^2\Delta G/NkT/\partial\phi_1^2)$ is observed. Extrapolating $(\partial^2\Delta G/NkT/\partial\phi_1^2)$ to zero yields the mean field-estimated spinodal temperature (see Figure 2). All estimated values for the spinodal temperatures are collected in Table 1 and presented in Figure 3.

The data thus indicate that at lower temperatures, the system becomes unstable again for composition fluctuations; i.e., the SANS data give experimental evidence for the existence of a ***narrow upper critical solution temperature (UCST) spinodal***

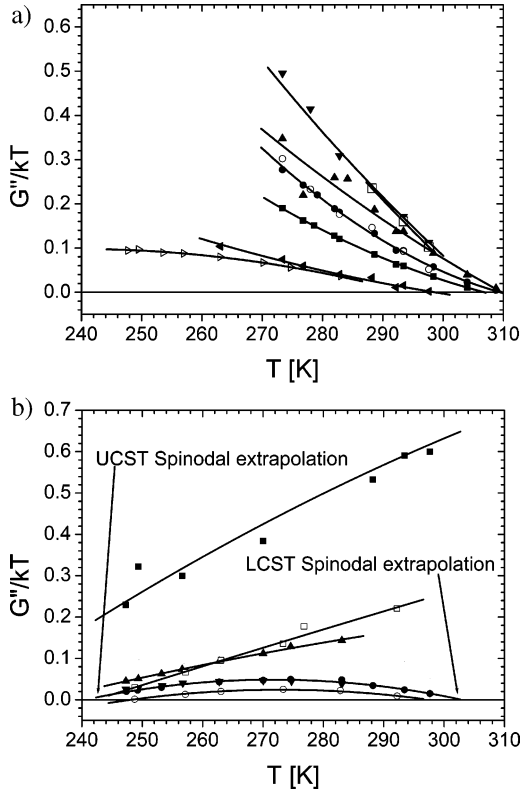

Figure 2. Plot of $(\partial^2\Delta G/(NkT))/\partial\phi_1^2$ vs T at given mixture composition. The extrapolated temperature at $(\partial^2\Delta G/(NkT))/\partial\phi_1^2 = 0$ is the spinodal temperature T_{spin}. The error bars are often smaller than the size of the symbols and are not shown. (a) $w_{PVME} = 0.70$: solid triangle pointing left; $w_{PVME} = 0.689$: open triangle pointing right; $w_{PVME} = 0.60$: ○; $w_{PVME} = 0.50$: □; $w_{PVME} = 0.40$: ▼; $w_{PVME} = 0.30$: ▲; $w_{PVME} = 0.20$: ●; $w_{PVME} = 0.10$: ■. (b) $w_{PVME} = 0.90$: ■; $w_{PVME} = 0.884$: □; $w_{PVME} = 0.844$: ▲; $w_{PVME} = 0.80$: ●; $w_{PVME} = 0.795$: ○; $w_{PVME} = 0.762$: ▼.

TABLE 1: Spinodal Temperatures T_{spin} Determined from the Extrapolation of $\partial^2\Delta G/(NkT)/\partial\phi_1^2$ vs T to Zero as a Function of the Mixture Composition

w_{PVME}	UCST T_{spin}/°C	w_{PVME}	LCST T_{spin}/°C
0.1	33.6		
0.2	36.3		
0.3	36.5		
0.4	33.8		
0.5	32.4		
0.6	30.5	0.6897	−88.2
0.6897	20.8	0.762	−36.7
0.7	25.3	0.7954	−25.1
0.762	28.8	0.8004	−32.7
0.7954	24.5	0.8492	−39.2
0.8004	29.6	0.8843	−31.0
0.9	-	0.9	−53.2
0.9384	-	0.9384	-

at high polymer compositions. This is in sharp contrast to the LCST that covers the whole composition interval. For several compositions, the extrapolated spinodal temperatures can only be considered to be very rough estimates in view of (i) the large span of the extrapolation and the limited number of available temperatures, and (ii) the extrapolated spinodal temperature is below the vitrification temperature of the studied mixture composition. For very high polymer concentrations, i.e., $w_{PVME} \geq 0.9$, we are certain that the spinodal temperature is lower than 250 K; below this temperature, we cannot get equilibrium measurements as the glass transition temperature intervenes. At the low concentration side, for $w_{PVME} \approx 0.68$, we only observe a leveling off in the value of $(\partial^2\Delta G/NkT/\partial\phi_1^2)$ with decreasing

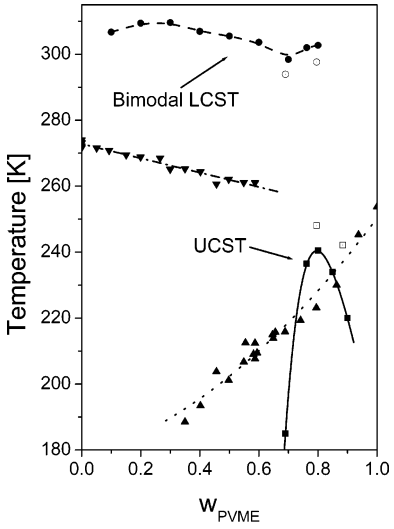

Figure 3. Temperature−composition phase diagram at atmospheric pressure of PVME/D_2O. Experimentally estimated LCST spinodal temperatures (●,○, - - - - -); experimentally estimated UCST spinodal temperatures (■,□, ——). Melting temperatures of D_2O (▼, -·-·-·) and the glass transition of PVME/H_2O (▲, ·····) as a function of composition (melting and glass transition temperatures are taken from literature and lines are drawn to guide the eye.[30]

temperature, and this mixture composition is certainly homogeneous to the lowest measured temperatures. Therefore, a very low spinodal temperature must be anticipated, and our rough estimate indicates that the spinodal temperature is again lower than the glass transition temperature of that mixture composition.

In Figure 3, two UCST (□) and two LCST spinodal temperatures (○) are the results for similar mixture compositions obtained in independent measurement sessions separated in time by more than one year. The $(\partial^2\Delta G/NkT/\partial\phi_1^2)$ data of this session that were used to obtain these spinodal temperatures are also shown in Figure 2b with open symbols. For instance, the data for $w_{PVME} = 0.796$ and $w_{PVME} = 0.8$ have the same course with temperature but are shifted along the vertical axis. Our suspicion is that this may have been due to a difference in the isotopic purity of the D_2O used on the two different occasions or differences in the amount of H_2O left in the pure PVME sample used in the mixture preparations. But in all cases, the SANS data convincingly show that at lower temperature, the system becomes unstable again for composition fluctuations. Despite the large extrapolations required to estimate the spinodal temperatures at the lowest and highest compositions and the large scatter on the extrapolated spinodal temperatures, the data give convincing proof of the existence of a ***narrow low-temperature UCST in PVME/D_2O mixtures***.

The SANS experiments give further evidence for ***UCST liquid−liquid phase separation***. For compositions and temperatures inside the narrow UCST spinodal gap, the SANS measurements yield scattering patterns indicative of heterogeneous structures. An example is provided in Figure 1b for $w_{PVME} = 0.762$ at $T = -42$ °C. Clearly, in the accessible q interval, we observe for $(\partial^2\Delta G/NkT/\partial\phi_1^2)$ versus q a q^{-4} dependence at small q (0.003 Å$^{-1} \leq q \leq$ 0.02 Å^{-1}), in line with the existence of defined interfaces (heterogeneous two-phase structure).[24] We are certain that in this instance, the q^{-4} dependence is related to liquid−liquid phase separation (i.e., strong segregation) and not related to the crystallization of D_2O from the concentrated mixture. Most importantly, for mixtures in this composition range, DSC experiments give no signal related to the crystallization or the melting of ice.[10,11,29] And for these high mixture

compositions and these low temperatures, we only observe a very weak optical opacity. The index of refraction difference between the two liquid phases is very small and/or the sizes of the coexisting phases are quite small and do not provide sufficient optical contrast to observe the phase separation very clearly, and the presence of crystalline D_2O would most likely lead to a higher optical contrast and higher turbidity.

The Amended Flory−Huggins Gibbs Energy of Mixing Expression. In an earlier analysis, SANS scattering cross sections were used to determine the parameters in a composition and temperature-dependent interaction function from the second-order compositional derivative of the extended F−H interaction parameter $g(\phi_1,T)$.[8,9,26] For these earlier experimental data only, a monotonic temperature dependence was observed, and a linear or reciprocal temperature dependence (eq 5b with either $g_{l1} = 0$ or $g_{l2} = 0$) was adequate to get an acceptable fit of the data. Now, including the new experimental data at higher concentrations, we need the full temperature function of eq 5b to describe the temperature dependence depicted in Figure 2. In the fitting procedure, large correlations occurred between the parameters occurring in eq 5, and we were unable to uniquely determine all the parameters. The current data set does not provide us with enough information to find out the complete polynomial dependence, and in fact, this will be impossible relying only on experimental data, as the crystallization of water always interferes in this composition range at the low polymer concentrations.

The Wertheim Lattice Thermodynamic Perturbation Theory. We, therefore, make a first attempt to understand the complicated phase behavior and the detailed information obtained from the SANS scattering experiments using a theoretical approach that incorporates directly and explicitly the formation of saturation interactions. As discussed in the Theory section, we follow the seminal work of Wertheim concerning saturation interactions mapped onto a lattice model to capture the essences of the saturation interactions that makes comparison with other theories developed for this purpose more feasible.

The predictions of the Wertheim lattice theory for a polymer solution involving saturation interactions between solvent molecules and between solvent molecules and polymer segments are presented. The theoretical spinodals and critical conditions are shown in the T*−ϕ_1 phase diagram in Figure 4a (and also 4b). The composition is given by the polymer site or volume fraction, ϕ_1, and the temperature is expressed in reduced temperature T^*. The parameters used for the calculations are summarized in Table 2 and were chosen to give a bimodal LCST at high temperature ($T^*_{crit} \approx 0.3$), which is a part of a closed-loop spinodal with the UCST top situated at $T^*_{crit} \approx 1.4$.

At sufficiently high temperatures, i.e., $T^* > 1.4$, the entropy dominates, and the system is, at all compositions, in a one-phase homogeneous state. As the temperature is decreased, the unfavorable dispersive interactions become important, and phase separation occurs, yielding a UCST miscibility gap ($T^*_{crit} \approx 1.4$), just as in the classic F−H theory. Upon further decreasing the temperature, the specific interactions between solvent and polymer start to become important, improving the miscibility in the system. This eventually results in re-entrant miscibility behavior and full miscibility over the whole composition range. For the selected parameter set, this occurs at about $T^*_{crit} \approx 0.3$.

A key factor for the occurrence of bimodal LCST miscibility gaps in the Wertheim LTPT is the relative strength of the solvent−solvent saturation interaction versus the solvent−polymer saturation interaction. Bimodality is only observed when the solvent−polymer strength is (somewhat) larger than

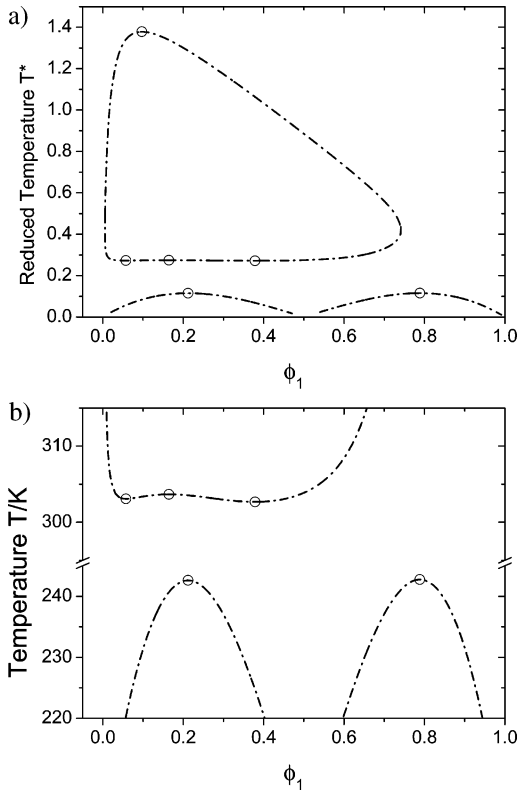

Figure 4. Theoretical reduced temperature−composition ($T^*-\phi_1$) phase diagram of model polymer solution. Predicted LCST spinodal curves (-·-·-·-) and critical conditions (○); parameters and values used in the predictions are summarized in Table 1. (a) Complete predicted phase diagram showing closed loop miscibility gap and adjacent UCST's. (b) Part of the predicted phase diagram zooming in on the bimodal LCST and the adjacent UCST's. The reduced temperature scale is converted to absolute temperature using eq 14.

TABLE 2: Parameter Values in the Wertheim LTPT Used to Calculate the Phase Behavior Depicted in Figure 4

parameter	value	parameter	value
s_1	100	K_{00}^{AA}	6
z	6	K_{11}^{BB}	6
ϵ_{01}/k	−0.1	$\Delta H_{m,0}^{0*}$	495
$\epsilon_{00}/k = \epsilon_{11}/k$	0	$T_{m,0}^{0*}$	1.500
ϵ_{00}^{AA}/k	1.5		0.200
			0.225
			0.250
$\epsilon_{00}^{AB}/k = \epsilon_{10}^{BA}/k$	2.8		

the solvent−solvent strength. In addition to the bimodal LCST phase behavior, at low temperatures, the occurrence is predicted of highly unconventional ***two narrow adjacent UCST miscibility gaps*** with their critical temperatures situated at ca. $T^*_{crit} \approx 0.12$. We will show in a future publication that the occurrence of high-temperature bimodal LCST phase behavior and low-temperature UCST phase behavior are closely connected.[16] At low temperatures, the saturation interactions between solvent and polymer are favored and are preferably "consumed" in a polymer−solvent association.

At the stoichiometric composition of the polymer−solvent associate ($\phi_1 = 0.5$), the favorable saturation interaction can be exploited optimally as all solvent and polymer molecules can be involved in these associations. Such complexes act then as a new component, and no liquid−liquid phase separation occurs, and the mixture remains homogeneous down to the lowest temperature. However, for off-stoichiometric compositions, one component is always in excess, and qualitatively, we can regard the polymer solution to consist of a polymer−solvent

associate (or complex) and molecules of component 0 or 1 depending on the overall composition. The component in excess can only have unfavorable dispersive interactions with the associate leading to the UCST miscibility gaps. Thus, the predicted adjacent UCST miscibility gaps arise from unfavorable dispersive interactions.

In the calculations, a 1:1 association between polymer segments and solvent molecules is predicted, which is the result of the specific model of saturation interactions used. In principle, we could use a more suitable saturation model to mimic the PVME/D_2O system more closely (for example, the solvent could be modeled using two donor and two acceptor sites, and the polymer repeating unit could be assigned two acceptor sites) and find appropriate parameters from the experimental data, giving a more accurate mapping of theory to experiment. Currently, our interest is focused on the bimodal LCST and the predicted adjacent UCST's. To link the theoretical results with the experimental phase behavior of PVME/water, the reduced temperature scale is mapped to the absolute temperature by assigning the theoretical LCST and UCST critical temperatures to the experimentally estimated LCST minimum and UCST maximum spinodal temperatures, viz. $T^* = 0.12 \leftrightarrow T = 240$ K and $T^* = 0.272 \leftrightarrow T = 303$ K, yielding the following relationships between reduced and absolute temperature:

$$T^* = -0.5181 + 0.00261T^*\ [\mathrm{K}] \text{ or } T\ [\mathrm{K}] = 198.51 + 383.14 \cdot T^* \quad (14)$$

From a purely theoretical point of view, this mapping procedure is not correct, as in principle, the mapping should be done by, e.g., fitting the theoretical phase behavior to the experimental data, providing estimates for the molecular parameters. Nevertheless, we pursue with this maneuver and look at some aspects of the theory that could help us in interpreting the experimental results in PVME/water. The result of this mapping is shown in Figure 4b, concentrating on the bimodal LCST-adjacent UCST region of the phase diagram.

The agreement between theory and experiment is not quantitative. For instance, the theoretical bimodal LCST spinodal is too narrow compared to the experimental one, the bimodality is not as explicit as observed in the experimental results, and the adjacent UCST are too broad and related to the existence of a strong association at 1:1 composition instead of the 1:2 composition found in PVME/water. However, the qualitative agreement between theory and experiments indicates that the theoretical model captures the essence of hydrogen-bonding interactions in these nonionic aqueous polymer solutions.

It must be remarked that to our knowledge, it is the first theory that is able to predict the bimodal phase behavior. Moreover, the existence of narrow adjacent UCST's are predicted. In fact, it are these predictions that motivated us to look closer at the low-temperature behavior employing SANS, and the experimental confirmation of a narrow UCST at high polymer compositions gives us confidence in the theory. We are unable to investigate directly the existence of a narrow UCST at low polymer compositions, as in this composition interval the crystallization of D_2O always intervenes. However, we conjecture here that the observation of peculiar crystallization behavior in PVME/water mixtures experimentally observed and discussed earlier[11] might very well be related to the existence of a UCST miscibility gap at polymer compositions $w_{PMVE} < 0.6$. The crystallization of water at low temperatures for a polymer mixture with $w_{PMVE} = 0.5$ was observed to proceed via the growth of "amorphous" looking spherulites consisting of small droplet-like structure. It is conceivable that the droplets are the result of liquid−liquid demixing via nucleation and growth upon entering the narrow UCST miscibility gap situated under the melting line of water at compositions $w_{PMVE} < 0.6$. The nucleation and crystallization of ice could then proceed in the dilute polymer phase at a much faster rate. Hence, the intriguing morphologies observed in PVME/water mixtures could be the result of a *UCST liquid−liquid nucleation and growth-assisted* crystallization process. However, so far we have no direct experimental evidence for this predicted low-temperature adjacent UCST.

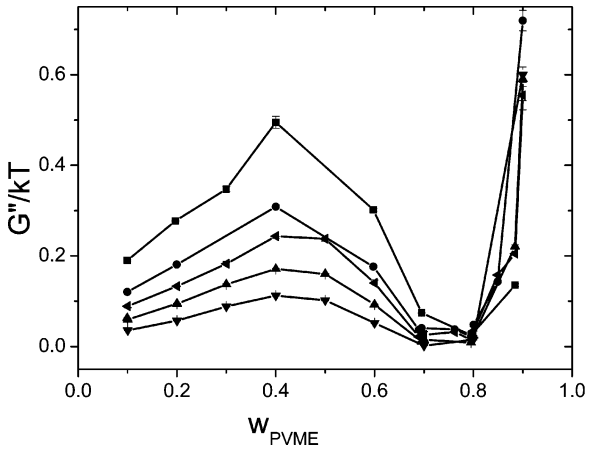

Figure 5. Plot of $\partial^2\Delta G/(\mathrm{NkT})/\partial\phi_1^2$ vs mixture composition at indicated temperatures. ($T = 273$ K: ■; $T = 283$ K: ●; $T = 288$ K: solid triangle pointing left; $T = 293$ K: ▲; $T = 298$ K: ▼).

Complex Formation in Concentrated Mixtures. Finally, we return to the issue of the formation of PVME/water complexes. The compositional curvature ($\partial^2\Delta G/NkT/\partial\phi_1^2$) is a quantitative measure for the average amplitude of the spontaneous thermal composition fluctuations $\langle\Delta\phi_{12}\rangle$ in the homogeneous mixture, and conversely, it is also a measure for the energy (in units of kT) required to create a concentration fluctuation of average amplitude $\langle\Delta\phi_{12}\rangle$.[8] The larger the value of ($\partial^2\Delta G/NkT/\partial\phi_1^2$), the smaller the amplitude of the spontaneous composition fluctuations becomes on average. In homogeneous mixtures with "normal" solution behavior, in which no complex formation occurs (e.g., solutions of polystyrene in cyclohexane), a typical concave dependence on mixture composition is found for ($\partial^2\Delta G/NkT/\partial\phi_1^2$), with large positive values at the extremes of the composition interval and reaching its minimum at some intermediate mixture composition. The high values at the extremes of the composition interval indicate that it becomes gradually more difficult for these concentrations to induce large composition fluctuations in a "normal" mixture, and in the pure component, only density fluctuations are possible; the scattered intensity due to concentration fluctuations is zero and, correspondingly, in this limit ($\partial^2\Delta G/NkT/\partial\phi_1^2$) becomes infinite.

The situation is quite different in PVME/water mixtures. In Figure 5, ($\partial^2\Delta G/NkT/\partial\phi_1^2$) is plotted as a function of composition at several temperatures for PVME/D_2O mixtures. Just as for "normal" solution behavior, the compositional curvature increases rapidly at very high polymer concentration, indicating that it becomes gradually more difficult to induce large composition fluctuations in these highly concentrated polymer mixtures. In Figure 5, the expected upswing at the dilute polymer side of the diagram is not observed because the smallest investigated polymer composition, $w_{PVME} = 0.1$, is not small enough to observe this phenomenon. However, interestingly and most importantly, ($\partial^2\Delta G/NkT/\partial\phi_1^2$) does not show the typical concave dependence expected for "normal" solution behavior

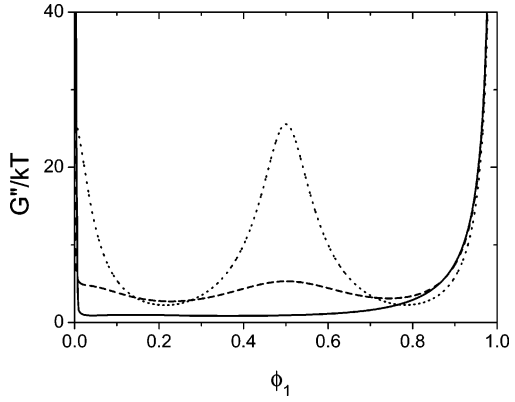

Figure 6. Plot of $(\partial^2\Delta G/(\mathrm{NkT}))/\partial\phi_1^2$ vs. mixture composition according to the Wertheim lattice thermodynamic perturbation theory at indicated temperatures: ($T^* = 0.25$ K, $T = 295$ *K*, −−); ($T^* = 0.2$ K, $T = 276$ K, - - - - - - -); ($T^* = 0.15$ K, $T = 256$ *K*, ·····).

but reaches a maximum in the composition interval $0.3 \leq w_{\mathrm{PVME}} \leq 0.5$. This indicates that, at these intermediate compositions, it again becomes more difficult to induce composition fluctuations. Thus, the experimental data reveal that at intermediate compositions, the amplitude of the thermal compositional fluctuations decreases.

The maximum value of $(\partial^2\Delta G/NkT/\partial\phi_1^2)$ is higher the lower the temperature, but notwithstanding this increase even at the lowest investigated temperature for the investigated compositions depicted in Figure 5, the energy needed to induce the fluctuations is just about $0.5 \cdot kT$. Thus, the clustering of water and PVME in this composition interval and at the investigated temperature is still small compared to the thermal energy. Therefore, it should be concluded that in the temperature interval considered in this study, the specific interactions between water/D_2O and PVME are still too weak to speak about the formation of a complex in the system. Nevertheless, the maximum value increases with decreasing temperature, and it is conceivable that at lower temperatures, a stable complex between water and PVME might be formed.

Considering the success of the Wertheim LTPT in the prediction of LCST and UCST phase behavior, it also worthwhile to look at the variation of the Gibbs energy curvature with composition and temperature as predicted by the Wertheim theory. In Figure 6, the variation of $(\partial^2\Delta G/NkT/\partial\phi_1^2)$ with composition at three selected values of the reduced temperatures are shown (the corresponding absolute temperatures according to the mapping of eq 14 are shown in the legend).

Just as for "normal" solution behavior, the compositional curvature increases rapidly at very low and very high polymer concentration, indicating that it becomes gradually more difficult to induce large composition fluctuations in these highly diluted or concentrated polymer mixtures. At sufficiently high temperature but below the bimodal LCST miscibility gap, the Gibbs curvature is almost like that of "normal" solution behavior (curve for $T^* = 0.25$). Upon decreasing the temperature at intermediate compositions, an increase in the compositional curvature is observed, indicating that it becomes gradually more and more difficult to induce regular composition fluctuations (curves for $T^* = 0.2$ and $T^* = 0.15$). Also, here in the prediction of the compositional curvature of the Gibbs energy, the agreement with the experimental data is gratifying and confirms that the theory is capturing the essential behavior of the system.

In Figure 7, the complete theoretical dependence of the compositional curvature as a function of temperature and composition is depicted. The $(\partial^2\Delta G/NkT/\partial\phi_1^2)$ scale runs from

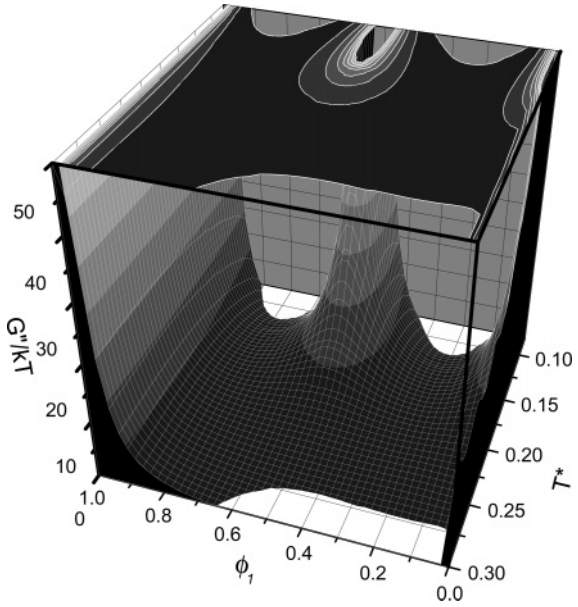

Figure 7. Plot of $(\partial^2\Delta G/(\mathrm{NkT}))/\partial\phi_1^2$ vs mixture composition according to the Wertheim lattice thermodynamic perturbation theory as a function of temperature and composition. The top surface is the contour plot of the underlying surface.

0 to 50. At $(\partial^2\Delta G/NkT/\partial\phi_1^2) = 0$, the spinodal is reached, and in the base plane of this figure, we also recognize the phase diagram depicted in Figure 3 (in Figure 7, the LCST is depicted in the front and the adjacent UCST at the rear side of the diagram, the polymer site fraction ϕ_1 runs from 1 to 0).

For temperatures even lower than $T^* = 0.15$, the adjacent UCST region is entered, and in the central homogeneous part centered around $\phi_1 = 0.5$, the Gibbs curvature increases further with decreasing temperature, and it can be assumed that the energy required to induce concentration fluctuations is so high that we can consider the polymer−solvent associate to act as a new independent component, showing density fluctuations instead of composition fluctuations. But at these very low temperatures, the low-temperature UCST's are present, and we can conclude that to have strong enough binding between the polymer and the solvent, so as to consider the polymer and solvent to form a stable complex, UCST phase separation should also occur. Hence, we may assume that at the experimental temperatures investigated for PVME/D_2O, the effect of the saturation interactions is not yet strong enough to consider the polymer/solvent association or complex completely stable.

For a truly stable complex solvent, crystallization cannot occur for mixture compositions higher than that of the composition of the complex, as it was suggested and discussed.[10] However, from the current calculations, we have strong indications that the occurrence of a strong associate or even complex in relation with the existence of a bimodal LCST at higher temperature must inevitably lead to the existence of adjacent UCST's *provided* that the closed miscibility loop at high temperature is the consequence of the interplay between unfavorable dispersive interactions and specific interactions. For these conditions, the existence of the low-temperature, adjacent UCST's is intimately related to the existence of a stable associate at these low temperatures. In fact, the existence of the UCST's implies the existence of the strong associate/complex and vice versa.

Conclusions

We have reported on SANS measurements for mixtures of PVME and D_2O in the homogeneous part of the phase diagram,

covering the whole composition range and focusing on the low-temperature behavior. The raw SANS data were treated according to fluctuation theory to obtain the absolute scattering cross section for concentration fluctuations. These data were fitted by the OZ equation, yielding the absolute scattering cross section in the forward direction and the OZ correlation length as a function of temperature and composition. The forward absolute scattering cross sections were converted into values for the compositional curvature of the Gibbs energy. Spinodal temperatures were determined from the experimental values of the compositional curvature of the Gibbs energy. The SANS data give experimental evidence for the existence of a ***narrow, low-temperature UCST*** in PVME/D_2O mixtures at high polymer compositions and for the occurrence of ***UCST liquid−liquid phase separation*** for compositions and temperatures inside the narrow UCST spinodal gap.

It turns out to be impossible to represent the experimental data together with earlier SANS data with an extended F−H interaction function depending on composition and temperatures. However, the experimental data are successfully interpreted in terms of the Wertheim LTPT for a polymer solution involving saturation interactions between solvent molecules and between solvent molecules and polymer segments. The phase behavior predicted with this model is very rich, and the theory is capable of predicting bimodal LCST phase behavior. A key factor for the occurrence of bimodal LCST phase behavior in the theory is the relative strength of the solvent−solvent saturation interaction versus the solvent−polymer saturation interaction. For certain values of the interaction parameters in the model, bimodal LCST phase behavior is observed, and at the same time, the occurrence of very peculiar UCST phase behavior at low temperatures is predicted. We will show in a future publication that the occurrence of high-temperature bimodal LCST phase behavior and low-temperature UCST phase behavior are closely connected.[16]

We also conjecture that the observation of the peculiar crystallization behavior in PVME/water mixtures experimentally observed and discussed earlier might very well be related to the existence of the low-temperature UCST miscibility gap at low polymer compositions.

Finally, the issue of the formation of PVME/water complexes was discussed. In the concentrated polymer mixtures, the scattering results do not provide evidence for strong complex formation. Even at the lowest investigated temperature, the energy needed to induce compositional fluctuations was found to be only ca. $0.5 \cdot kT$, and in the temperature interval considered in this study, the specific interactions between water/D_2O and PVME are too weak to bring about the formation of a complex in the system.

Also in the prediction of the compositional curvature of the Gibbs energy, the Wertheim LTPT gives excellent qualitative agreement with experiment, and the theory captures the essential behavior of the system. The current calculations indicate that the occurrence of a strong associate or even complex in relation with the existence of a bimodal LCST at higher temperature must inevitably lead to the existence of adjacent UCST's**.** In fact, the existence of the UCST's implies the existence of the strong associate/complex and vice versa.

Acknowledgment. We thank the Dutch Science Foundation (NWO) for financial support in the application for beam time at ISIS. The work was supported by the bilateral (international) scientific and technological cooperation of the Ministry of the Flemish Community and the Ministry of Science and Technology of the People Republic of China (BIL01/06). We thank the Funds for Scientific Research Flanders (FWO) for financial support. L.T. is indebted to the Katholieke Universiteit Leuven for a postdoctoral fellowship (OT 03/93).

References and Notes

(1) Schaefer-Soenen, H.; Moerkerke, R.; Berghmans, H.; Koningsveld, R.; Dusek, K.; Solc, K. *Macromolecules* **1997**, *30*(3), 410−416.
(2) Maeda, Y.; Mochiduki, H.; Yamamoto, H.; Nishimura, Y.; Ikeda, I. *Langmuir* **2003**, *19*(24), 10357−10360.
(3) Walker, J. S.; Vause, C. A. *Proc. Symp.Thermophys. Prop.* **1982**, *8*(1), 411−418.
(4) Dormidontova, E. E. *Macromolecules* **2002**, *35*(3), 987−1001.
(5) Panayiotou, C.; Sanchez, I. C. *Macromolecules* **1991**, *24*(23), 6231−6237.
(6) Tanaka, F. *Polym. J. (Tokyo)* **2002**, *34*(7), 479−509.
(7) Tanaka, H. *AIP Conf. Proc.* **1992**, *256*(Slow Dyn. Condens. Matter), 238−239.
(8) Nies, E.; Ramzi, A.; Berghmans, H.; Li, T.; Heenan, R. K.; King, S. M. *Macromolecules* **2005**, *38*(3), 915−924.
(9) Solc, K.; Dusek, K.; Koningsveld, R.; Berghmans, H. *Collect.Czech. Chem. Commun.* **1995**, *60*(10), 1661−1688.
(10) Meeussen, F.; Bauwens, Y.; Moerkerke, R.; Nies, E.; Berghmans, H. *Polymer* **2000**, *41*(10), 3737−3743.
(11) Zhang, J.; Berge, B.; Meeussen, F.; Nies, E.; Berghmans, H.; Shen, D. *Macromolecules* **2003**, *36*(24), 9145−9153.
(12) Maeda, Y. *Langmuir* **2001**, *17*(5), 1737−1742.
(13) Maeda, H. *J. Polym. Sci., B: Polym. Phys.* **1994**, *32*(1), 91−97.
(14) Wertheim, M. S. *J. Stat. Phys.* **1984**, *35*, 19−34.
(15) Wertheim, M. S. *J. Stat. Phys.* **1984**, *35*, 35−47.
(16) Nies, E. In preparation.
(17) Heenan, R. K.; King, S. M. Large Scale Strutures. http://www.isis.rl.ac.uk/largescale/loq/loq.htm, 2003.
(18) King, S. M.; Heenan, R. K. Sample Environments. http://www.isis.rl.ac.uk/largescale/LOQ/technical/tech_spec.htm, 1−1−1995.
(19) King, S. M.; Heenan, R. K. Using COLETTE. http://www.isis.rl.ac.uk/largescale/loq/documents/colette.pdf, 1−1−1995.
(20) Chu, B. *J Chem Phys* **1963**, *41*(1), 226−234.
(21) Smoluchowski, M. *Ann. Phys. (Berlin)* **1908**, *25* 205.
(22) Einstein, A. *Ann. Phys. (Berlin)* **1911**, *33*, 1275−1298.
(23) Debye, P. *J Chem Phys* **1959**, *31*, 680−687.
(24) Higgins, J. S.; Benoit, H. C. *Polymers and Neutron Scattering*; Oxford University Press: New York, 1994.
(25) King, S. M. Small-angle Neutron Scattering. In *Modern Techniques for Polymer Characterization*; Pethrick, R. A., Dawkins, J. V., Eds.; Wiley: UK, 1999; Chapter 7, pp 171−232.
(26) Koningsveld, R.; Stockmayer, W. H.; Nies, E. *Polymer Phase Diagrams: A Textbook*; Oxford University Press: New York, 2001.
(27) Flory, P. J. *J. Chem. Phys.* **1942**, *9*, 660.
(28) Huggins, M. L. *J. Chem. Phys.* **1942**, *9*, 440.
(29) Zhang, J.; Teng, H.; Zhou, X.; Shen, D. *Polym. Bull. (Berlin)* **2002**, *48*(3), 277−282.
(30) Van Durme, K.; Loozen, E.; Nies, E. L. F.; Van Mele, B. *Macromolecules* **2005**, *38*, 10234−10243.